Vis Comput (2009) 25: 863–871
DOI 10.1007/s00371-009-0316-6

ORIGINAL ARTICLE

Consistent parameterization and statistical analysis of human head scans

Pengcheng Xi · Chang Shu

Published online: 3 March 2009

Abstract Statistical shape analysis of 3-D scanned human heads provides important information for many applications. Nevertheless, special geometry processing techniques have to be developed for consistently parameterizing scans due to the fact that different scanning projects vary in landmark definition, noise control and other factors. For consistent parameterization, fitting a generic model to each scan has proved to be an effective method. In this paper, improved techniques are presented to solve problems in parameterizing different data sets. Principal Component Analysis (PCA) is thus conducted on the consistently parameterized data sets, and shape variances along principal components are demonstrated. In addition, shape variations analyzed by Independent Component Analysis (ICA) are also presented.

Keywords Consistent parameterization · 3D mesh deformation · Principal component analysis · Independent component analysis

1 Introduction

The recent development of 3-D imaging technology allows capture of 3-D shapes of humans with reasonable accuracy and efficiency. This capability has been demonstrated in a few anthropometry surveys in which large numbers of human shapes were digitized. The earliest large-scale survey is the CAESAR project (CAESAR–Civilian American and European Surface Anthropometry Resource), where 5000 full-body scans were performed in North America and Europe [1]. Another example is the SizeChina[1] project, where 2000 head scans were carried out at six locations in China. These scanning projects have collected an enormous amount of information about the human shape and have potential impacts on a variety of applications, such as ergonomic design, medical research, and computer animation and gaming.

The detailed information about the human shape provided by the 3-D data can be used to study the variations of it within a population and compare the changes in shape across different populations. Formerly, shape variation was studied in Statistical Shape Analysis [2] where sparse landmarks that correspond to anatomical feature locations were used on all individuals of the database [3]. The 3-D scans enable the study of shape variation using dense point sets, which can reveal detailed shape change. It also gives more intuitive visualization of the shape variation.

However, performing statistical analysis on dense surface data poses new challenges. In order to build a statistical model, the data has to be parameterized, which means a dense point-to-point correspondence among data models has to be established. Raw scan data are noisy and often incomplete due to occlusions inevitably occurring in the scanning process; therefore, much geometry processing is necessary.

In this paper, we present techniques for parameterizing the scan data. We focus on analyzing the head and face shape data, motivated by two types of applications: design of headgear such as helmets and face masks, and diagnosis of genetic diseases. The design of headgear requires detailed information of human head shape, but most of today's

P. Xi (✉) · C. Shu
Institute for Information Technology, National Research Council Canada, Ottawa, Canada
e-mail: pengcheng.xi@nrc-cnrc.gc.ca

C. Shu
e-mail: chang.shu@nrc-cnrc.gc.ca

[1] www.sizechina.com.

head-related products are designed using simple 1-D measurements, like head length, width or circumference. The 3-D scans capture the surface of the human head and face and thus make it possible to design products that fit humans better. Certain genetic diseases, like the Williams syndrome, have been shown to have special characteristics in the shape of the face [4, 5]. Studying facial morphology using 3-D scans would help diagnose this kind of disease in the early stages.

The key to a high quality statistical model for the 3-D data is an accurate registration or parameterization that brings the data models into correspondence. 3-D anthropometry scans usually start with putting markers or landmarks on the subjects prior to scanning. These landmarks, corresponding to stable anatomical positions that reside on every person, can only be located by palpating the subjects. Formerly, these landmarks have been used to measure the linear dimensions on the human body; in fact they are the only measurements in traditional anthropometry. For 3-D surface shape analysis, landmarks can be used to guide the deformation of a template model for each data scan and thus register the scans. Although it is tedious and time-consuming to put landmarks on human subjects, it is so far the only reliable way of getting corresponding points across a population. Landmark-free approaches exist [6–8], but their accuracy and reliability for critical applications has yet to be proven.

Unfortunately, the scanning process has not been standardized, and thus data collected from different scanning projects vary in landmark definition, noise level, information loss, and mesh resolution. This poses problems for registering large data sets robustly. In this paper, we discuss specific techniques that handle these problems using three large data sets: CAESAR (using only the head part of the full-body scan), SizeChina, and a Canadian scanning project. Figure 1 shows examples of typical scans from the three data sets. Since we only use the head part of the data, the CAESAR data set is low-resolution (around 20 K triangles) and has only a few landmarks. The SizeChina data set is high-resolution (about 600 K triangles) and has more landmarks on the face, but the cap only covers part of the head, introducing noise from scanning the dark hair. The Canadian data set is also high-resolution (around 300 K triangles), but only has landmarks on face.

Our contributions include: an estimation of virtual landmarks on the back of the head, which helps improve the parameterization of the Canadian and SizeChina data sets; surface characteristics found on hair and cap tops, which is a solution to dealing with noise, especially in the SizeChina data set; PCA and ICA on parameterized data sets, which bring about a clear understanding of the 3-D shape variations.

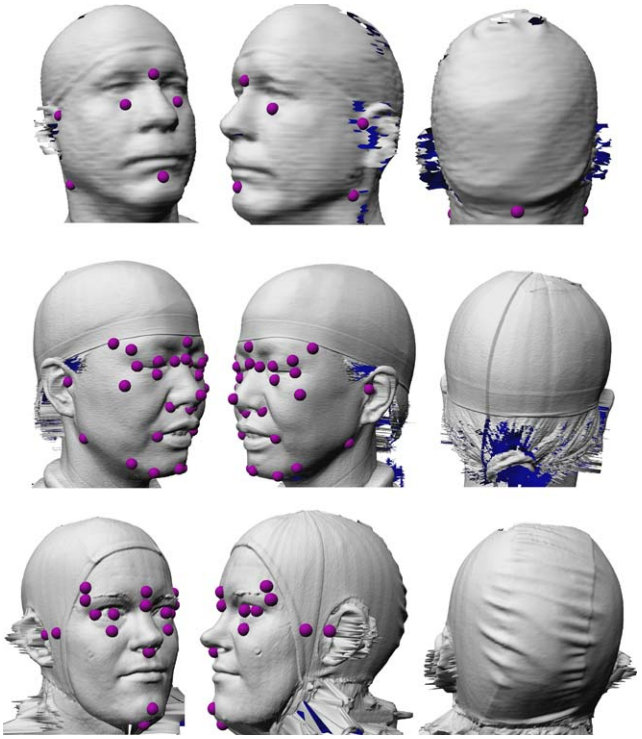

Fig. 1 Landmark definitions on sample scan data in CAESAR (*first row*), SizeChina (*second row*), and a Canadian scanning project (*third row*)

2 Literature review

A representative work on modeling the variations of human body shape is by DeCarlo et al. [9]. The authors described a system that was capable of automatically generating distinct, plausible face geometries. This was an early work on anthropometrical statistics for likely face measurements.

Blanz and Vetter's work [10] is a milestone for human modeling and reconstruction. It explores two key problems of computer-aided face modeling. First, new face images or new 3D face models can be registered automatically by making a large number of comparisons with an internal model. Second, the approach regulates the naturalness of the modeled faces and avoids those with an unnatural appearance. This work successfully incorporates statistical approaches into computer graphics to obtain visual information from a given database.

For human bodies, a robust matching technique is introduced in [11]. It is based on an energy-minimization framework, and is similar to that of Marschner et al. [12]. Instead of using the surface smoothness term in [12], the authors in [11] tried to minimize variation of the deformation itself. This keeps localized warping stable so that the whole surface gets little deformation.

Our parameterization work [13] has applied Radial Basis Functions (RBFs) to human body scans to speed up the deformation process. RBF for elastic alignment was first used

in [14] where intermediate objects were constructed, given two or more objects of general topology. Another RBF-based approach is from [15], where the correspondence between dense surfaces was computed by volume morphing with RBF, followed by cylindrical projection.

After consistent parameterization, the meshes correspond well in features and are therefore ready for statistical shape analysis. Principal components analysis is a popular, unsupervised, statistical method to find useful model representations. In PCA, any given model can be decomposed as a linear combination of standard basis models ('principal components'). Independent components analysis is a statistical technique that represents a multidimensional random vector as a linear combination of non-Gaussian random variables ('independent components') that are as independent as possible.

This paper is organized as follows: Sect. 3 focuses on parameterization of human heads utilizing RBF to deform a generic head model, and introduces several improvements on parameterization of different data sets; Sect. 4 addresses PCA and a constrained ICA on the consistently parameterized head models; discussions and conclusions are made in Sect. 5.

3 Consistent parameterization

This section starts with the introduction of consistent parameterization based on Radial Basis Function (RBF) [13], then proceeds to solving specific problems in parameterizing head scans from different scanning projects.

3.1 Consistent parameterization

The template-based consistent parameterization includes first a rough but quick deformation on a generic model utilizing RBF, and then a fine fitting with an error-minimization scheme.

3.1.1 Radial basis function network

The deformation function for the RBF network is entirely built on landmarks. With a number of landmarks in both the generic model and target surfaces, good interpolation is ensured. Because Fig. 1 demonstrates that landmark definitions differ in quantity and location, we need to identify landmarks on the generic model, and have them correspond to those on target scans in each scanning project. The generic model also needs to be customized so that the resolution resembles that of the target scans. These settings are made only once for each scanning project and remain unchanged during the batch parameterizations.

An RBF network can be stated as an interpolation: let $p_i \in \Re^3$ and $q_i \in \Re^3, i = 1, \ldots, n$, be two sets of n landmarks, which serve as the input. The source landmarks p_i lie on the generic model and target landmarks q_i correspond to features on the target surface. Three RBF networks, one for each coordinate, are established to build the mapping:

$$q_i = f(p_i), \quad i = 1, \ldots, n. \tag{1}$$

Since this function is defined over the volume spanned by the landmarks, it can be used to deform all vertices on the whole surface. This mapping can then be expressed by a radial basis function, i.e. a weighted linear combination of n basic functions defined by the two sets of landmarks:

$$f(p_i) = \sum_{j=1}^{n} w_j \Phi_j(p_i). \tag{2}$$

When computing the mapping coefficients, input points will be the landmarks and when doing the deformation, input points will be the vertices of the influence region of certain landmarks from the generic model.

This linear system is solved using a standard LU decomposition with pivoting. After training and computing the weight vector, new positions of these non-feature vertices are calculated using this RBF network from their initial positions. The RBF transformed model maintains the same topology as the generic model.

In the mapping defined by (1), there are several radial functions, which can be applied for model deformation. Thin-plate spline, multi-quadrics and Gaussian functions have been tested to find the best solution. By comparing these three radial basis functions, we find that the Gaussian function has the best performance for our data sets. The Gaussian function is defined as:

$$\Phi_j(r) = \exp\left(-r^2/c^2\right), \tag{3}$$

where c is the only parameter. Through experiments we have found $c = 0.1$ works well.

The RBF transformation is a quick way of deforming the generic model close to the target model in shape and orientation (Fig. 2(c)). It is then followed by a nonlinear optimization process to further fine tune the registration.

3.1.2 Fine registration

After the rough transformation, the distance between the deformed generic model and the target is greatly reduced. The error definitions in [11] are therefore simplified to two: (a) the difference between the source surface and target surface (data error) and (b) the difference between transformations on neighboring vertices (smoothness error). Because RBF

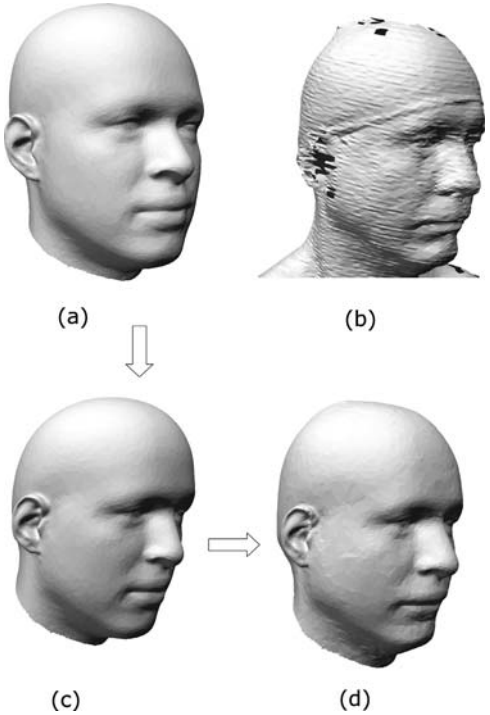

Fig. 2 Parameterization process for CAESAR data: (**a**) generic head model (with 22 K triangles), (**b**) target scan, (**c**) deformed generic model with RBF, (**d**) deformed generic model after fine fitting

ensures good registration of landmarks, we do not need to consider them in the fine tuning step.

Suppose the transformed generic model is U, and the scanned target surface is Γ. For each vertex on U, we define a 4×4 transformation matrix T_i. Each vertex has 12 degrees of freedom to define the transformation. Our intent is to find a set of transformations that move each vertex to its closest point on Γ. This process needs to be repeated a few times in order to align the RBF-transformed generic model to the target surface.

The evaluation of these repetitions depends on two errors: data error and smoothness error. Data error is defined as:

$$E_d = \sum_{i=1}^{m} \text{dist}^2(T_i v_i, \Gamma), \tag{4}$$

where m is the number of non-marker vertices in U, and dist() function computes the distance between a vertex on U and its closest vertex on Γ.

Smoothness error is defined as:

$$E_s = \sum_{\{i,j|\{v_i,v_j\}\in \text{edges}(U)\}} \|T_i - T_j\|^2. \tag{5}$$

The smoothness error is not defined for the smooth surface but for the actual deformations applied to the generic model. The diffusion process of transformations extends this deformation to neighboring vertices. The definition of smoothness error minimizes the deformation over the template surface and thus prevents adjacent parts of the template surface from becoming aligned to disparate parts of the target surface.

The overall error is defined as a weighted sum of these two errors:

$$E = aE_d + bE_s, \tag{6}$$

where a and b are two weights and subject to the constraint $a + b = 1$.

By setting two different weights for data and smoothness error, and by minimizing the overall error, we get the fine mapping results in Fig. 2(d).

3.2 Customized parameterization

3.2.1 Virtual landmarks

The approaches from [11, 13] both rely on landmarks to drive the deformation of generic models. In human head-scanning projects, it is easy to locate landmarks on the face where rich geometric features are available, but there is more difficulty locating landmarks on the back of the head due to the smoothness of the skull. In the three databases introduced, only the CAESAR data set has one landmark defined on the back of the head, and thus the scheme introduced in Sect. 3.1 suffices for parameterization of the CAESAR heads.

For the SizeChina and Canadian Scanning data sets, we rely on a subset of the markers from the front of the head to estimate the location of a virtual landmark in the back. As shown in Fig. 3, we calculate the intermediate location P_{middle} between the landmark on the left ear P_{left} and that on

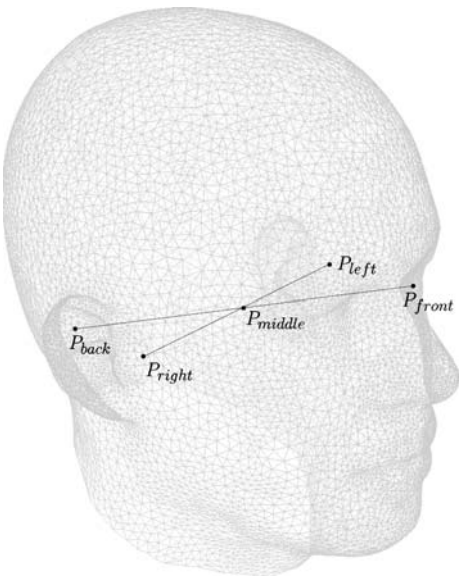

Fig. 3 Calculation of a virtual landmark

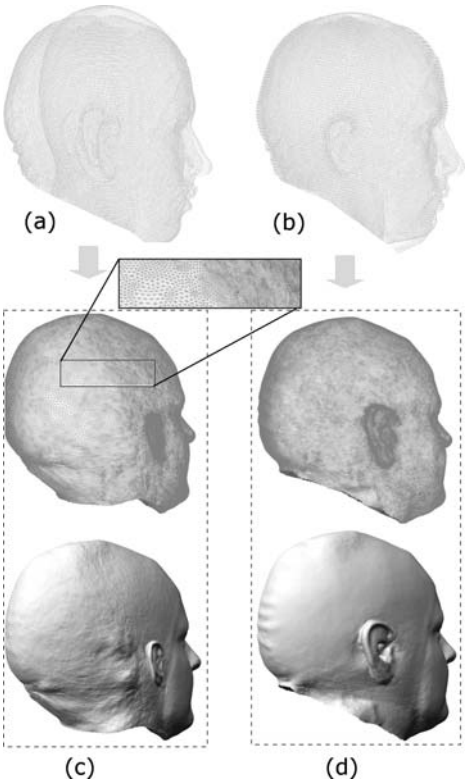

Fig. 4 (**a**) comparison of RBF-deformed generic model and a target scan without calculation of virtual landmarks; (**b**) comparison of RBF-deformed generic model and a target scan utilizing virtual landmarks; (**c**) mesh structure and flat shading of the generic model after fine fitting from (**a**); (**d**) mesh structure and flat shading of the generic model after fine fitting from (**b**)

the right ear P_{right}, draw a direct line from the landmark on the forehead P_{front} through the intermediate location P_{middle} towards the back of the head, and find an intersecting vertex P_{back} on the back as the virtual landmark. The virtual landmark will be used only once in guiding the rough deformation of the generic model, and will not be used during the fine fitting as it does not represent an actual feature.

With the virtual landmark, we are able to create a natural shape after applying the RBF. As shown in Fig. 4, the virtual landmark in the back helps deform the generic model much closer to the target shape, thus speeding up the fine fitting and maintaining a regular mesh structure.

3.2.2 Labeling patches on the generic model

In parameterizing the SizeChina data set, we also found most female subjects did not fully cover their hair during the scanning. This poses another problem of properly representing the actual head shape. Figure 5 demonstrates that the hair scan is less smooth than the face, neck and most of the other parts of the head scan.

Because the fitting process consists of finding a nearest neighbor v_i^1 on the target scan for each vertex v_i, we can

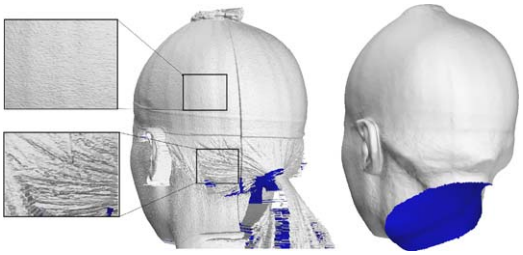

Fig. 5 Parameterization result before improvement (noise from cap and hair is mistakenly reconstructed as real shape of the head; left is the target scan and its zoomed-in view on the cap and the hair; right is the parameterization result before any improvement is done)

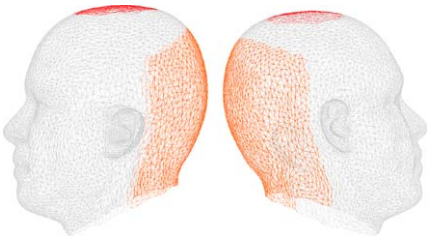

Fig. 6 Selection of top and back of the generic head for a lower-weight deformation

stop the current vertex v_i from moving towards v_i^1, if the v_i^1 is detected to be noise; therefore, we need to traverse through the target scan to find those v_i^1, because they are unreliable in representing the target shape.

A flag scheme is thus introduced to mark each vertex on the target surface. In particular, we label vertices on a triangle, if the dihedral angle between it and its neighbor is greater than a threshold. We also label vertices at the boundaries of the mesh holes. Suppose f_1 is the flag for each vertex on the target model, it thus can have two possible values: '1' when this vertex is located on a triangle with a large dihedral angle to a neighbor, or when this vertex is located on a boundary of a hole; or '0' for all the other vertices.

Another flag is defined on the generic model. In parameterizing the SizeChina data set, we select the top and back of the generic model as shown in Fig. 6. Define flag f_2 for each vertex on the generic model, it thus has two possible values: '1' when this vertex lies right on the selected patches; or '0' for all the other vertices.

The scaling factor w_i for each vertex in the generic model is thus defined as:

- $f_1 = 0$ and $f_2 = 0$: $w_i = 1.0$;
- $f_1 = 0$ and $f_2 = 1$: $w_i = 0.1$;
- $f_1 = 1$ and $f_2 = 0$: $w_i = 0.1$;
- $f_1 = 1$ and $f_2 = 1$: $w_i = 0.01$.

With the new flagging scheme, we achieve an improvement on parameterizing the female subject data. The new parameterization result is shown in Fig. 7, where the top and back of the head are smoothed.

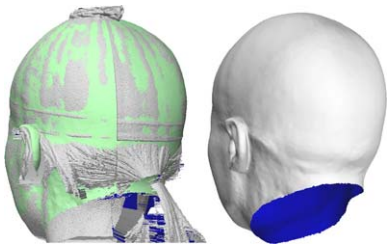

Fig. 7 Parameterization result after incorporating a flag scheme

4 Analysis of parameterized models

Once the scan models are parameterized, statistical shape analysis can be conducted to find out the shape variations. Because of its simplicity, Principal Component Analysis is the most commonly used method. For certain applications, Independent Component Analysis is also useful. In this section, we present results of both PCA and ICA. All experiments used the CAESAR data set.

Representing each shape as a vector x_i, and putting all the m_1 vectors into a matrix $X = (x_1, x_2, \ldots, x_{m_1})$, a covariance matrix $\text{cov}(X) = \sum (x_i - \overline{x})(x_i - \overline{x})^T$ is calculated, where $\overline{x}$ is the average of all the x_i. An eigen-decomposition on the covariance matrix creates $(m_1 - 1)$ principal components, which are organized in columns to create a new matrix Φ.

Our analysis on 260 consistently represented head models (approximately half are males and the other half are females) creates a sequence of principal components. Therefore we can traverse along each component and observe the shape variances, five of which have been shown in Figs. 8–12. In each figure, we put in the first row three flat-shading models representing the shapes by selecting component weights from $-3\sigma_i$, to zero, then to $3\sigma_i$, where the σ_i is squared root of the ith eigen value calculated from the eigen decomposition. We also put the three models in a single space and show them in point clouds but from profile and frontal views, in the second row of each figure.

Figure 8 shows in flat shading and in point cloud the shape variations along the first principal component. It demonstrates a change from a male subject to a female and the head size decreases. The second component has a variation on the forehead and the neck, as shown in Fig. 9. Figure 10 presents variation along the third component, in which the head changes from a round shape to a long narrow one.

Figure 11 and Fig. 12 show the models along the fourth and fifth principal components. Both have large variations on the head shape, despite the fact that the face also makes distinctive changes.

Given m training data, theoretically the same number of independent components can be calculated; however, there will be too much work and the variances will become imperceptible. Because the original training data can be approximated by a linear combination of the principal components, the same number of independent components can be derived by performing an ICA on the selected principal components [16].

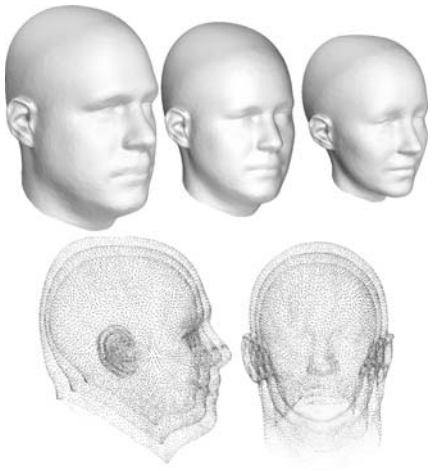

Fig. 8 Shape variation along the first principal component

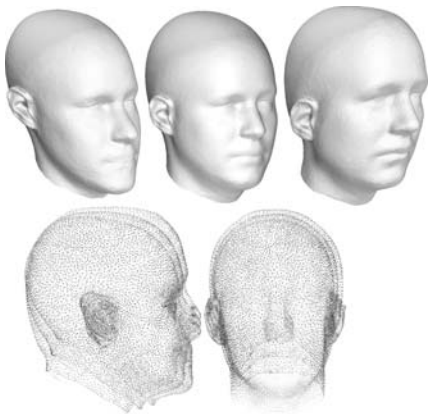

Fig. 9 Shape variation along the second principal component

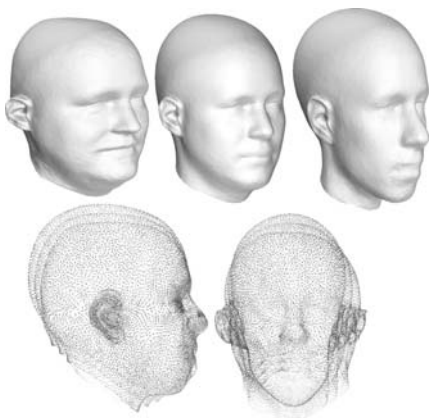

Fig. 10 Shape variation along the third principal component

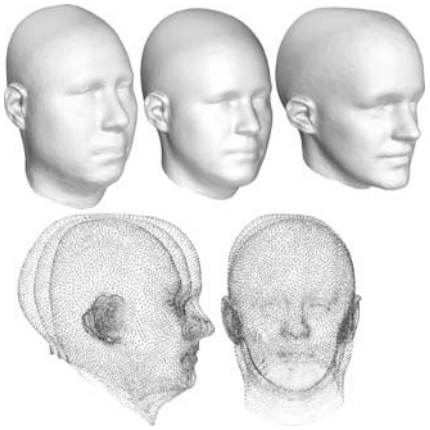

Fig. 11 Shape variation along the fourth principal component

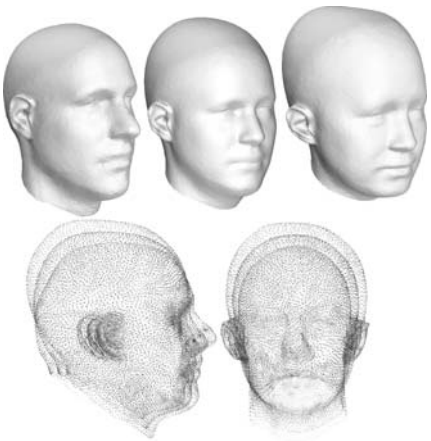

Fig. 12 Shape variation along the fifth principal component

After conducting the ICA, we observe the variations along the independent components, as shown in Figs. 13–17. The first component corresponds mainly to the shape changes of the lower head, as can be observed from the point cloud models in Fig. 13. Figure 14 shows the main shape changes on the face and the back of the head. We find the variation along the third independent component (shown in Fig. 15) is of great similarity to that of the second principal component. Figure 16 presents a growth in the shape of the head, which is observed along the third independent component. Finally, a shape change in the face from long and narrow to round is observed in Fig. 17.

Besides the similarity between the second PC and the third IC, there is also a finding that the variation along the third PC can be reconstructed by changing the face shape with the fifth IC, by reshaping the neck with the first IC, and by growing top of the head with the fourth IC. Head shape change on the first PC can be made by using the change along the first IC for neck resizing, and using the change along the fourth IC for top of the head. Following the same principle, the fourth PC is a combination of the third and

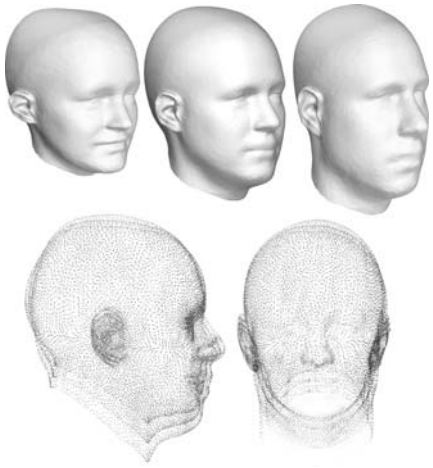

Fig. 13 Shape variation along the first independent component

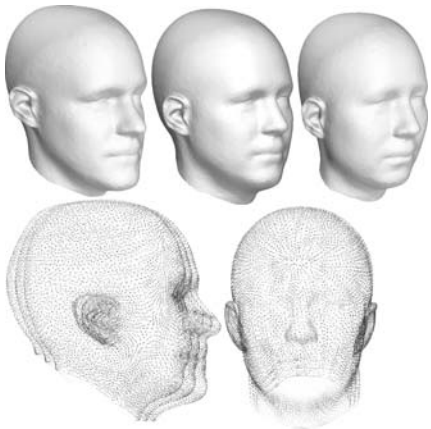

Fig. 14 Shape variation along the second independent component

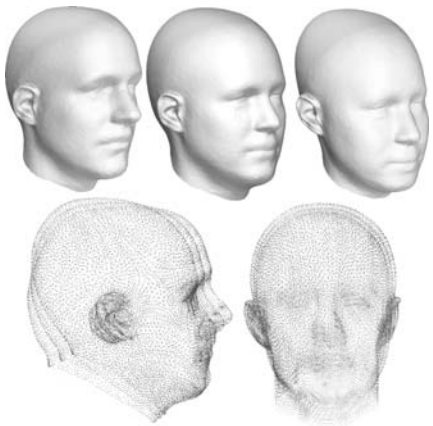

Fig. 15 Shape variation along the third independent component

the fourth IC, as the third IC enlarges the back of the head and the fourth IC helps enlarge the top of the head. A comparatively weaker connection between the fifth PC and the

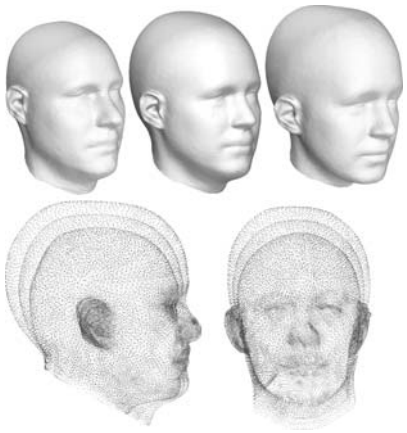

Fig. 16 Shape variation along the fourth independent component

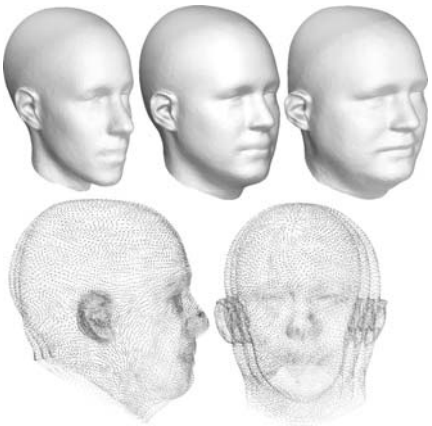

Fig. 17 Shape variation along the fifth independent component

third IC mainly on facial appearance and back-of-head shape change is also observed.

5 Discussions and conclusions

We had to customize the parameterization approach in [11, 13] to head scans from the SizeChina and the Canadian data sets, because there were insufficient numbers of landmarks. For the reason that RBF is mainly landmark driven, the deformed generic model tends to go towards the front of the face and leaves the side, e.g. the ears, and the back of the head distorted. Introducing the virtual landmark solves the problem. Our experiments also showed that, a multi-resolution approach, as introduced in [11], brings about better results on the SizeChina and the Canadian data sets than a single-resolution approach does; however, this does not make a difference on the parameterization of the CAESAR head scans.

Of the 260 principal components, variance along the first five principal components constitutes about 76.6 percent of all the variations in the training data set. Due to space limitation, we can only discuss the first few variations on principal components and on corresponding independent components. Despite this limitation, the comparison does show results of great interest by finding the relationship between the principal components and the independent components. There are equally important usages for principal components and independent components; in specific circumstances, one can be of more usage than the other. Therefore requirements in specific circumstances will decide which analysis is to be conducted. Although the authors in [17] introduced ICA on human faces for speech animation, and [18] presented results on human torsos, to our knowledge, this is the most detailed analysis on head shape variation.

An accurate parameterization on raw scanned data makes statistical analysis results reliable for various applications. PCA and ICA on head scans helps build shape spaces, which have many potential applications including product design, virtual character creation, face recognition, and detection of pathologic shapes.

Acknowledgements The authors would like to thank Pierre Meunier for providing the Canadian data set, and Prof. Roger Ball for providing the SizeChina data set. We appreciate the inputs from Prof. WonSook Lee. We also acknowledge comments on our work from the anonymous reviewers.

References

1. Robinette, K., Daanen, H., Paquet, E.: The CAESAR project: A 3-D surface anthropometry survey. In: Proc. 2nd International Conference on 3D Digital Imaging and Modeling (3DIM'99), pp. 380–386 (1999)
2. Dryden, I.L., Mardia, K.V.: Statistical Shape Analysis. Wiley, New York (1998)
3. Bookstein, F.L.: Morphometric Tools for Landmark Data: Geometry and Biology. Cambridge University Press, Cambridge (1997)
4. Hammond, P., Hutton, T., Allanson, J., Campbell, L., Hennekam, R., Holden, S., Patton, M., Shaw, A., Temple, I.K., Trotter, M., Murphy, K., Winter, R.: 3D analysis of facial morphology. Am. J. Med. Genet. **126A**, 339–348 (2004)
5. Hutton, T., Buxton, B., Hammond, P., Potts, H.: Estimating average growth trajectories in shape-space using kernel smoothing. IEEE Trans. Med. Imaging **22**(6), 747–753 (2003)
6. Dekker, L., Douros, I., Buxton, B.F., Treleaven, P.: Building symbolic information for 3D human body modeling from range data. In: Proceedings of the Second International Conference on 3-D Digital Imaging and Modeling (3DIM'99), Ottawa, Canada, pp. 388–397 (1999)

7. Ben Azour, Z., Shu, C., Mantel, A.: Automatic locating of anthropometric landmarks on 3D human models. In: Third International Symposium on 3D Data Processing, Visualization and Transmission (3DPVT 2006), pp. 750–757 (2006)
8. Russ, T., Boehnen, C., Peters, T.: 3D face recognition using 3D alignment for PCA. In: Computer Vision and Pattern Recognition (CVPR'06), pp. 1391–1398 (2006)
9. DeCarlo, D., Metaxos, D., Stone, M.: An anthropometric face model using variational techniques. In: ACM SIGGRAPH Computer Graphics Proceedings, pp. 67–74 (1998)
10. Blanz, V., Vetter, T.: A morphable model for the synthesis of 3D faces. In: ACM SIGGRAPH Computer Graphics Proceedings, pp. 187–194 (1999)
11. Allen, B., Curless, B., Popović, Z.: The space of human body shapes: reconstruction and parameterization from range scans. ACM Trans. Graph. **22**(3), 587–594 (2003)
12. Marschner, S.R., Guenter, B., Raghupathy, S.: Modeling and rendering for realistic facial animation. In: Proceedings of 11th Eurographics Workshop on Rendering, pp. 231–242 (2000)
13. Xi, P., Lee, W.-S., Shu, C.: Analysis of segmented human body scans. In: Proceedings of the Graphics Interface Conference, pp. 19–26 (2007)
14. Cohen-Or, D., Solomovic, A., Levin, D.: Three-dimensional distance field metamorphosis. ACM Trans. Graph. **17**(2), 116–141 (1998)
15. Noh, J.Y., Neumann, U.: Expression cloning. In: Proceedings of SIGGRAPH, pp. 277–288 (2001)
16. Bartlett, M., Movellan, J.R., Sejnowski, T.J.: Face recognition by independent component analysis. IEEE Trans. Neural Netw. **13**(6), 1450–1464 (2002)
17. Kalberer, G.A., Mueller, P., Gool, L.V.: Speech animation using viseme space. In: Proceedings of the Vision, Modeling, and Visualization, pp. 463–470 (2002)
18. Ruto, A., Lee, M., Buxton, B.: Comparing principal and independent modes of variation in 3-D human torso shape using PCA and ICA. In: Proceedings of ICA Research Network International Workshop, University of Liverpool, pp. 101–104 (2006)

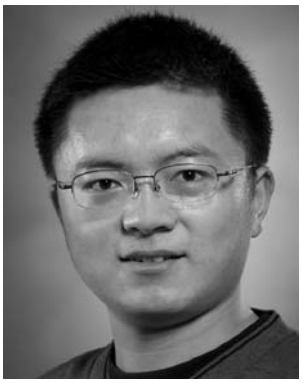

Pengcheng Xi received the Master's Degree in Computer Science from the University of Ottawa, Canada, in 2007. After that he started working at the Institute for Information Technology, National Research Council of Canada (NRC). He conducts research and development in digital human modeling, including consistent parameterization, statistical shape analysis, and knowledge-based applications.

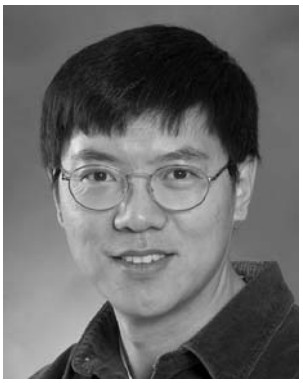

Chang Shu received the Ph.D. in Computer Science from the Queen Mary College, University of London, UK, in 1992, and the B.Sc. in Computer Science from Harbin Institute of Technology, China, in 1985. He is currently a senior research scientist at the Institute for Information Technology, National Research Council of Canada (NRC). He is also an adjunct research professor at the School of Computer Science, Carleton University, Ottawa, Canada. From 1992 to 1996, he was a research associate in the Department of Mechanical and Aerospace Engineering at the Carleton University. From 1996 to 1998, he was a research scientist at the Integrated Manufacturing Technologies Institute of the NRC. His primary research interests include geometry processing for imaging and graphics, statistical shape analysis, and the application of digital human modeling in ergonomic design, animation, and biomedical research.